Gold nanorings as substrates for surface-enhanced Raman scattering

Mohamad G. Banaee* and Kenneth B. Crozier

School of Engineering and Applied Sciences, Harvard University, Cambridge, Massachusetts 02138, USA
**Corresponding author: mbanaee@seas.harvard.edu*

Received December 11, 2009; accepted January 11, 2010;
posted January 29, 2010 (Doc. ID 121333); published February 26, 2010

Surface-enhanced Raman scattering using gold nanoring substrates is studied. The measured enhancement factors of arrays of single nanorings and nanoring dimers are compared with that of an array of nanodisk dimers. The measured average enhancement factor for the single nanorings is 4.2×10^6. The experimental enhancement factors are compared with the electromagnetic enhancement factors predicted by simulations.

OCIS codes: 240.6680, 240.6695.

The field enhancement around nanoscale metallic particles offers an efficient tool to manipulate light–matter interactions at optical frequencies [1]. For spectroscopic applications, the field confinement around these structures reduces the mismatch between the wavelength of the incident light and size of the molecules under study. In the surface-enhanced Raman scattering (SERS), this can boost the Raman cross section of molecules by many orders of magnitude. SERS offers a very sensitive tool for biological and chemical sensing [2], enabling vibrational spectra to be obtained even from single molecules [3]. The signal enhancement in SERS mostly comes from the excitation of localized surface plasmon resonances (LSPRs) and the "lightning rod" effect [4]. The latter is particularly pronounced for sharp tips and nanoparticle dimers with small gaps.

The optimum substrate for SERS should have the highest average field enhancement possible, be highly tunable, and offer a broad resonance bandwidth, although satisfying all these criteria is very challenging. One of the candidates for a highly tunable substrate is the ring geometry. The optical properties of gold nanorings fabricated by colloidal lithography were reported by Aizpurua *et al.* [5]. They showed that the LSPR frequency strongly depends on the ratio of the thickness to ring outer radius. This tunability, which is similar to that of nanoshells [6], allows tuning of the plasmon resonances from visible to near-IR wavelengths via reducing the ring thickness. The reduced amount of the metal in the ring geometry compared to disks of the same radius results in smaller absorption loss. We report here a study of SERS using metal nanorings, the first experimental report, to the best of our knowledge.

Fabricating metallic rings with high-resolution methods such as electron beam lithography enables us to have great control of the periodic arrangement of the nanoparticles. Moreover, the ring geometry has an advantage over the nanoshell pattern in that molecules can attach to the inner wall as well as the outer wall, which is beneficial as substantial field enhancement occurs there. In addition to the conventional SERS, studying the field confinement in metallic rings could also have applications in optical corrals [7] and lasing spacers [8].

In this study, we carry out SERS measurements on benzenethiol monolayers formed on gold rings, ring dimers, and disk dimers. By comparing SERS signals obtained from these samples with those measured from a solution of neat benzenethiol, SERS enhancement factors (EFs) are determined. Using numerical electromagnetic simulations, we find the electric fields on the surfaces of structures. This allows us to simulate the electromagnetic EF. The experimental results are compared with these simulations.

The starting substrate is a glass microscope slide coated with a layer of indium tin oxide (ITO) with a thickness of 20 nm (Sigma Aldrich). The patterns are defined in the poly(methyl methacrylate) (PMMA) by electron beam lithography with a dose of 900 $\mu C/cm^2$ and an acceleration voltage of 100 kV (Elionix ELS7000). A gold layer (30 nm thick) is deposited following development, and lift-off is performed using acetone. Scanning electron microscope (SEM) images of the resulting ring dimer and ring arrays are shown in Fig. 1. The nanoparticles are arranged in two-dimensional arrays with lattice constants of 500 nm along the y axis (dimer axis) and 300 nm along the x axis. The inner and outer diameters of the rings are, on average, 60 and 100 nm, respectively. The gap width of the ring dimers is on average 25 nm.

Numerical electromagnetic simulations are performed by the finite-difference time-domain method. A plane wave illuminates the periodic structure from the air side at normal incidence. A Cartesian grid with a spacing of 1 nm along x, y, and z directions is used. The refractive indices of the glass substrate and the ITO layer on it are taken to be 1.45 and 1.65 [9], respectively. The gold permittivity is modeled by a Lorentz–Drude expression whose parameters are

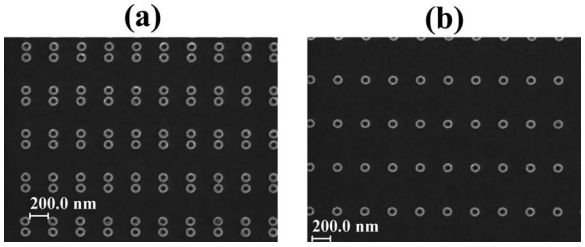

Fig. 1. SEM images of arrays of gold (a) ring dimers and (b) rings.

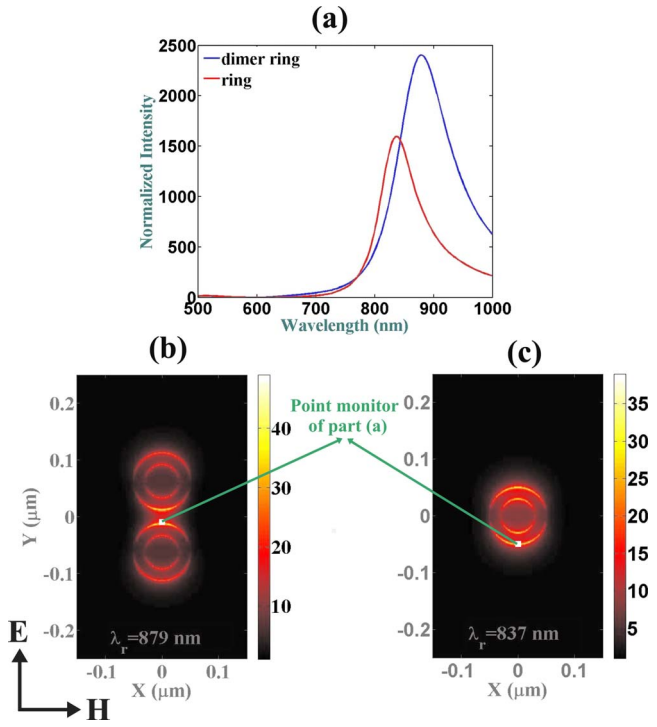

Fig. 2. (Color online) (a) Electric field intensity ($|E|^2$) enhancement versus wavelength for a monitor point on the nanostructure surface. Normalized field ($|E|$) distribution on surfaces of (b) ring dimer and (c) ring structures.

chosen to match the experimentally determined permittivity [10]. The geometries of the simulated nanoparticles are chosen to match those of the fabricated structures, as given above.

In Fig. 2, the results of the electromagnetic simulations are shown. In Fig. 2(a), intensity enhancement as a function of wavelength is plotted for rings and dimer rings. The intensity enhancement is defined as the intensity at a monitor point on the nanoparticle surface divided by the intensity that would occur at the same point in the absence of the nanoparticle. The monitor point is chosen on the top surface of the ring, on its outer edge. From Fig. 2(a), it can be seen that the resonances are at 837 and 879 nm for the ring and ring dimer, respectively. In Figs. 2(b) and 2(c), field ($|E|$) distributions are plotted for the rings and ring dimers illuminated at the plasmon resonance frequencies.

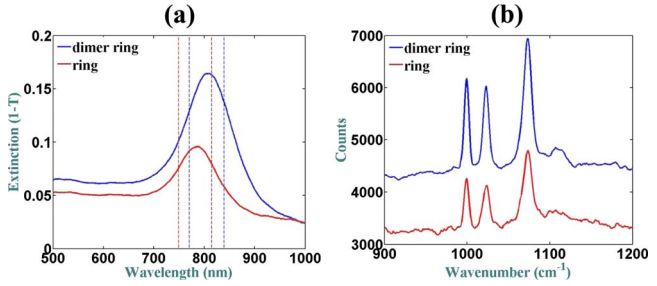

Fig. 3. (Color online) (a) Measured extinction spectra and (b) SERS spectra for ring and ring dimer structures. The vertical dashed lines in (a) show the locations of the laser wavelengths (749 nm for the ring and 770 nm for the ring dimer patterns) and the Stokes Raman signal of benzenethiol at 1074 cm^{-1}.

To measure the plasmon resonance spectrum of the fabricated structures, white light transmission spectroscopy is performed. Light from a xenon lamp is collimated and polarized along the dimer axis and impinges on the sample at normal incidence. The power transmitted through the array is measured and normalized by the power transmitted through an unpatterned region of the substrate. In Fig. 3(a), we plot the measured extinction spectrum, given by $1-T$. The peaks in the spectrum correspond to the LSPRs and are 787 and 810 nm for the ring and ring dimer structures, respectively. These are in reasonable agreement with the predictions of simulations, with the deviations that could be due to differences in geometry and optical constants.

For SERS measurement, self-assembled monolayers of benzenethiol are formed on the gold nanostructures. Figure 3(b) shows SERS measurement from the ring and ring dimer samples. SERS measurement is carried out with a confocal Raman system (Renishaw inVia Raman microscope). A cw Ti:sapphire laser, polarized along the dimer axis, is focused on the sample using an objective lens (NA of 0.4). The laser wavelengths are 749 and 770 nm for the ring and ring dimer structures, respectively. The laser power incident on the sample is ~0.8 mW, and the signal acquisition time is 10 s. The vertical dashed lines in Fig. 3(a) show the locations of the laser wavelengths and the Stokes Raman signal of benzenethiol at 1074 cm^{-1}.

To compare SERS enhancements of ring and ring dimer structures with the disk dimers, similar steps are taken for the fabrication, simulation, and measurement of the latter. The fabricated structure is shown in Fig. 4(a). The disk diameter is 170 nm, and the gap spacing is 25 nm. In Fig. 4(b), we plot the near-field intensity enhancement simulated for a monitor point on the disk top surface adjacent to the

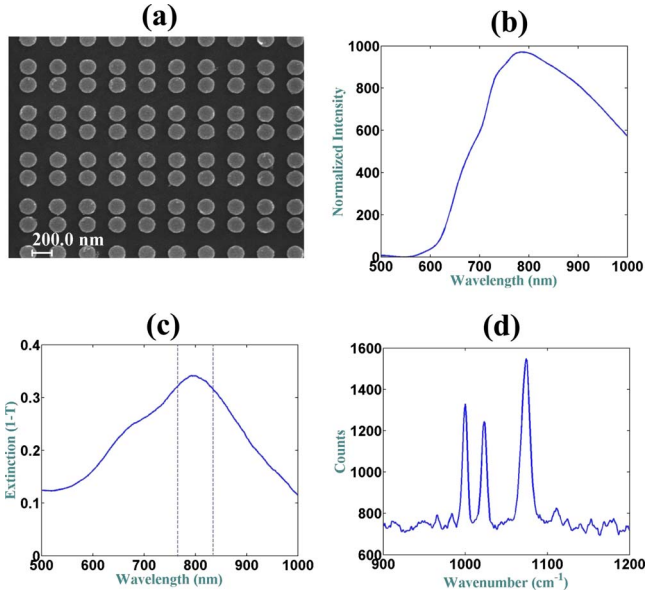

Fig. 4. (Color online) (a) SEM image, (b) simulated near-field intensity enhancement, (c) measured extinction spectrum, and (d) SERS spectrum of the disk dimer structures. The laser wavelength (766 nm) and 1074 cm^{-1} benzenethiol vibrational mode are shown as dashed lines in (c).

Table 1. Comparison between Calculated Average SERS Enhancement and Experimental Values for Ring, Dimer Ring, and Dimer Disk Patterns

Pattern	$\lvert E_{\max}\rvert^4$	$(\lvert E(\lambda_r)\rvert^4)_{\text{ave}}$	$(\lvert E(\lambda_l)\rvert^2 \lvert E(\lambda_s)\rvert^2)_{\text{ave}}$	SERS Measurement
Ring	2.3×10^6	1.8×10^5	5.3×10^4	4.2×10^6
Dimer ring	5.8×10^6	2.2×10^5	1.1×10^5	3.9×10^6
Dimer disk	9.2×10^5	3.5×10^4	2.9×10^4	5.8×10^5

gap. The measured extinction spectrum is shown in Fig. 4(c). In Fig. 4(d), SERS spectrum is shown, obtained with a laser wavelength of 766 nm.

To determine the experimental EF in SERS, we compare the Raman signals measured on the nanostructured substrates with that from a neat benzenethiol solution, taking into account the number of molecules in each case [11]. To determine the number of molecules on the nanostructured substrates, we multiply the surface area (top, inner, and outer wall surfaces) by the surface packing density of benzenethiol on gold. This is taken as 6.8×10^{18} molecules/m^2, the largest packing density reported in the literature [12]. The experimental SERS EFs for 1074 cm^{-1} line of benzenethiol for all patterns are shown in the last column of Table 1. SERS EFs of the ring and dimer ring have the same magnitude, and they are roughly seven times higher than the dimer disks. In addition, SERS EF of the ring structures is slightly higher than that of the ring dimers. From electromagnetic modeling (Fig. 2), we would not expect this to be the case, since the field enhancement at resonance is higher for ring dimer structures. We found out that due to the proximity effect a small fraction of the ring dimers are partially filled with gold, which could cause the decrease in the EF of this geometry with respect to the ring structure.

From the numerical electromagnetic modeling results, the simulated electromagnetic EFs can be found. In the second column of Table 1, the fourth powers of the peak field enhancements ($\lvert E\rvert^4$) at resonance are given. To find the total SERS electromagnetic EF that models our experiment, however, we must average the electromagnetic EF over the nanostructure surface. The measured EF is an average value over a broad distribution of EFs on the substrate [13]. In the third column of Table 1, we calculate the average electromagnetic EF by taking it as the fourth power of the electric field enhancement at the plasmon resonance frequency of each structure, averaged over the exposed nanoparticle surfaces. This method implicitly assumes that the laser and Stokes lines are at the same frequency. To get a better prediction of the EF, the case in which the laser and Raman signal (at 1074 cm^{-1}) are equally separated about the resonance is also considered. The fourth column in Table 1 shows the results of this method. It can be seen that the measured SERS EFs are 1 or 2 orders of magnitude larger than the simulated electromagnetic EFs. The mismatch between the EFs in the experiment and the simulation is possibly due to chemical enhancement and the role of roughness of the fabricated structures providing additional enhancement. Indeed, the magnitude of the difference is consistent with previous discussions of the chemical mechanism accounting for $\sim 10-10^2$ of the total Raman enhancement [14].

In summary, SERS in ring and ring dimer geometries is studied. The result is compared with SERS from disk dimers. Although the peak field enhancement for ring dimers is found to be higher than that of rings through simulations, the measured SERS EFs are very similar (3.9×10^6 and 4.2×10^6). These are approximately seven times higher than that measured for disk dimers.

This work was supported by Schlumberger–Doll Research and the Defense Advanced Research Projects Agency (DARPA). Fabrication was carried out at the Harvard Center for Nanoscale Systems, which is supported by the National Science Foundation (NSF). We thank Eric Diebold, Dr. Paul Peng, and Professor Mazur (Harvard University) for the use of their Raman spectrometer.

References

1. L. Novotny, Nature **455**, 887 (2008).
2. K. Kneipp, M. Moskovits, and H. Kneipp, *Surface-Enhanced Raman Scattering: Physics and Applications* (Springer, 2006).
3. J. A. Dieringer, R. B. Lettan II, K. A. Scheidt, and R. P. Van Duyne, J. Am. Chem. Soc. **129**, 16249 (2007).
4. J. H. Kang, D. S. Kim, and Q-H. Park, Phys. Rev. Lett. **102**, 093906 (2009).
5. J. Aizpurua, P. Hanarp, D. S. Sutherland, M. Kall, G. W. Bryant, and F. J. Garcia de Abajo, Phys. Rev. Lett. **90**, 057401 (2003).
6. C. E. Talley, J. B. Jackson, C. Oubre, N. K. Grady, C. W. Hollars, S. M. Lane, T. R. Huser, P. Nordlander, and N. J. Halas, Nano Lett. **5**, 1569 (2005).
7. Y. Babayan, J. M. McMahon, S. Li, S. K. Gray, G. C. Schatz, and T. W. Odom, ACS Nano **3**, 615 (2009).
8. N. I. Zheludev, S. L. Prosvirnin, N. Papasimakis, and V. A. Fedotov, Nature Photon. **2**, 351 (2008).
9. R. A. Synowicki, Thin Solid Films **313–314**, 394 (1998).
10. A. D. Rakic, A. B. Djurisic, J. M. Elazar, and M. L. Majewski, Appl. Opt. **37**, 5271 (1998).
11. E. C. LeRu, E. Blackie, M. Meyer, and P. G. Etchegoin, J. Phys. Chem. C **111**, 13794 (2007).
12. C. M. Whelan, M. R. Smyth, and C. J. Barnes, Langmuir **15**, 116 (1999).
13. Y. Fang, N. Seong, and D. D. Dlott, Science **321**, 388 (2008).
14. T. H. Reilly, S. Chang, J. D. Corbman, G. C. Schatz, and K. L. Rowlen, J. Phys. Chem. C **111**, 1689 (2007).